# Scale-free networks emerging from multifractal time series

Marcello A. Budroni,[1,*] Andrea Baronchelli,[2] and Romualdo Pastor-Satorras[3,†]
[1]*Nonlinear Physical Chemistry Unit, Faculté des Sciences, Université libre de Bruxelles (ULB), CP 231-Campus Plaine, 1050 Brussels, Belgium*
[2]*Department of Mathematics-City, University of London-Northampton Square, London EC1V 0HB, United Kingdom*
[3]*Departament de Física, Universitat Politècnica de Catalunya, Campus Nord B4, 08034 Barcelona, Spain*
(Received 19 December 2016; published 16 May 2017)

Methods connecting dynamical systems and graph theory have attracted increasing interest in the past few years, with applications ranging from a detailed comparison of different kinds of dynamics to the characterization of empirical data. Here we investigate the effects of the (multi)fractal properties of a signal, common in time series arising from chaotic dynamics or strange attractors, on the topology of a suitably projected network. Relying on the box-counting formalism, we map boxes into the nodes of a network and establish analytic expressions connecting the natural measure of a box with its degree in the graph representation. We single out the conditions yielding to the emergence of a scale-free topology and validate our findings with extensive numerical simulations. We finally present a numerical analysis on the properties of weighted and directed network projections.

DOI: 10.1103/PhysRevE.95.052311

## I. INTRODUCTION

Network science [1] has emerged in recent decades as a transverse interpretative framework for understanding the structure and phenomena that takes place on them, ranging from financial crises and traffic congestion to epidemic and social influence spreading [2–4].

In the realm of dynamical systems [5], network techniques have been applied to the analysis of nonlinear time series, with a particular focus on characterizing chaotic dynamics [6]. The main idea of this methodology is to project the information of a time series into the topology of a network. The key element of this approach resides in the identification of nodes and links in the network from the time series information. Several alternatives have been proposed in this context [7]. Thus, Zhang and Small [8] consider cycles of a pseudoperiodic time series as the nodes of a network, which are connected by links depending on the similarity between cycles. Lacasa *et al.* [9,10], on the other hand, build on the concept of *visibility graphs*, where nodes correspond to series data points and two nodes are connected if a straight line can be established between them without intersection with any intermediate data height.

Another general approach is based on encoding topological information from the reconstructed phase space of a time series into a *proximity network*. In these networks, nodes represent segments of time series or vectors in the related reconstructed phase space, and links depend on a specific criterion determining adjacency in the phase space. Cycle networks [11], correlation networks [12,13], and recurrence networks [14–17] are typical examples of proximity networks. Finally, the related class of *transition networks* [18–21] encompasses different models for mapping time series into networks, in which the values on the time signal are mapped into a finite number of states (regions in the phase space of the series), representing the nodes, which are connected if the signal transits from one state to another one. This transformation procedure preserves the temporal information of the dynamics in the network, is stable to noise affecting real time series, and can account for the fundamental structure of the related attractors [21].

Using this kind of network projections, several aspects of dynamical systems have been cast in terms of topological network properties. Here we will focus in particular on the effects that the *fractal* and *multifractal* properties of a time signal have on the topology of representative classes of projected networks. Many time signals, particularly those arising from a chaotic or strange attractor [6], have a fractal structure, characterized by a statistically self-similar pattern in the phase space. Moreover, they can also show multifractal properties, described by a strongly heterogeneous probability of visiting different neighborhoods of the phase space [22–25]. Using as a simple example an undirected binary transition network representation [19,26], framed within a box-counting formalism [23] in which each box corresponds to a vertex, we find analytic expressions tying the visitation probability of a box with its associated degree. From these relations we obtain the conditions under which an undirected projected network grows with a scale-free topology [27], characterized by a degree distribution of the form $P(k) \sim k^{-\gamma}$. Our results highlight the correspondence between an attractor's structure and the topology of the associated projected network and relate the possible origin of a heterogeneous scale-free topology with the heterogeneous and hierarchical visitation probability characterizing multifractal attractors.

The present paper is organized as follows: In Sec. II, we briefly summarize the multifractal formalism for chaotic time series and attractors. In Sec. III, we present an undirected transition network mapping for general time series, based on the box-counting algorithm [19]. In Sec. IV, we relate the topological properties of the associated undirected networks with the multifractal properties of the original time series. This relation is directly mediated by the natural measure of the series, defined as the probability that the time sequence visits a given box in a partition of the topological support of the series. Numerical checks of our theoretical predictions are

*mbudroni@ulb.ac.be
†romualdo.pastor@upc.edu

 

detailed in Sec. V. In Secs. VI and VII, we consider and study numerically the extension of the network representation in terms of weighted and directed networks, respectively. Finally, we present our conclusions in Sec. VIII.

## II. MULTIFRACTAL TIME SIGNALS

For time signals arising from strange (chaotic) attractors, it is common that different regions of the phase space are differently visited, and chaotic orbits spend most of their time in a small region of the geometrical support underneath the chaotic attractor itself. This heterogeneity is at the basis of the so-called multifractal structure of the strange attractor, which can be mathematically captured by the formalism presented below [22,24].

Let us consider a real-time signal, or a $d$-dimensional chaotic attractor, given by the normalized sequence of points $\mathcal{G} = \{\vec{x}_t : \vec{x}_t \in [0,1]^d, t = 1,2,\dots n\}$, where the index $t$ represents either time or the order in the sequence of points that generate the attractor (e.g., the index of the iteration in an iterated map), while $n \gg 1$ is the number of points in the signal. We consider a partition of the set $[0,1]^d$ in $M$ boxes of length $\varepsilon = M^{-1/d}$. Box are labeled by the indexes $i$, with $1 \leqslant i \leqslant M$. Let us associate to each point $\vec{x}_t = \{x_t^{(1)}, x_t^{(2)}, \dots, x_t^{(d)}\}$ in the sequence an integer index

$$i_t = 1 + \sum_{r=1}^{d} \lfloor x_t^{(r)} L \rfloor \, L^{r-1} \tag{1}$$

in the range $1 \leqslant i_t \leqslant M$, where $L = M^{1/d}$, and $\lfloor z \rfloor$ is the floor function. In this sense, the signal or attractor can be interpreted as visiting the $i_t$th box in the partition at time $t$. In heterogeneous fractals, not all the boxes will be equally visited. In general, during the $n$ steps of the signal, the $i$th box will be visited a number of times $n_i$, and the total number of boxes visited at least once will be $N(\varepsilon)$. This quantity coincides with the number of boxes of length $\varepsilon$ needed to cover the fractal set, and thus we can define the box or capacity dimension of the attractor [23], $D_0$, by the relation

$$N(\varepsilon) \sim \varepsilon^{-D_0}. \tag{2}$$

Let us define the probability $p_i(\varepsilon) = \lim_{n\to\infty} n_i/n$, termed the *natural measure*, as the probability that the chaotic map visits the $i$th box of the $N(\varepsilon)$ available during an infinitely long orbit. For an homogeneous structure in $d$ dimensions, $p_i(\varepsilon) \sim \varepsilon^d$, while in the case of a uniform fractal of dimension $D_0 \leqslant d$, $p_i(\varepsilon) \sim \varepsilon^{D_0}$. In more complex situations, however, the attractor exhibits a nonuniform fractal distribution, and we assume a general form for the natural measure $p_i(\varepsilon) \sim \varepsilon^{\alpha_i}$, where the exponent $\alpha_i$, taking values in the interval $[\alpha_{\min}, \alpha_{\max}]$, measures the strength of the local singularity of the measure at box $i$. In general, there will be many boxes with the same value of $\alpha$, such that their number scales as $N_\alpha(\varepsilon) \sim \varepsilon^{-f(\alpha)}$. The function $f(\alpha)$, called the multifractal spectrum of the measure, defines the fractal dimension of the set of boxes with the given value $\alpha$, and is in general a convex function with a single maximum. An equivalent, and numerically simpler, description can be obtained from the generalized dimensions $D_q$, defined as [22]

$$D_q = \frac{1}{q-1} \lim_{\varepsilon\to 0} \frac{\log \sum_i p_i(\varepsilon)^q}{\log \varepsilon}, \tag{3}$$

which, for $q \geqslant 0$, fulfill $D_0 \leqslant D_q \leqslant D_\infty \equiv \alpha_{\min}$. For a uniform measure $D_q = \text{const.} = D_0$. For multifractal measures, $D_q$ is a decreasing function of $q$, which is related with the multifractal spectrum $(\alpha, f(\alpha))$ by means of a Legendre transformation [22], defining a parametric exponent $\alpha(q)$ that fulfills the equations

$$\alpha(q) = \frac{d}{dq}(q-1)D_q, \tag{4}$$

$$f(\alpha(q)) = q\alpha(q) + (1-q)D_q. \tag{5}$$

Numerically, the generalized dimensions can be estimated from Eq. (3), by noticing that, for finite $\varepsilon$,

$$\sum_i p_i(\varepsilon) \sim \varepsilon^{(q-1)D_q}, \tag{6}$$

allowing $D_q$ to be determined from a linear regression of $\sum_i p_i(\varepsilon)$ for decreasing values of $\varepsilon$ (increasing $M$) in a log-log plot.

## III. NETWORK MAPPING

In order to construct an undirected unweighted transition network representation, we follow the approach in Refs. [19,26] and associate a (virtual) vertex to each box $1 \leqslant i \leqslant M$ in the partition of the chaotic attractor in phase space. Actual vertices in the network are given by the set of boxes that have been visited at least once by the signal, with a size $N(\varepsilon)$. Edges in the network are established by associating an undirected connection between vertices $i$ and $i'$ if the signal jumps at least once between boxes $i$ and $i'$ in two consecutive time steps, i.e., $i \equiv i_t$ and $i' \equiv i_{t+1}$ or $i' \equiv i_t$ and $i \equiv i_{t+1}$ during its orbit.

The resulting projected networks, which are characterized by the coarse-grained scale $\varepsilon$, are connected by construction, and preserve temporal information of the generator of the signal. A completely random, stochastic signal will lead to a fully connected network; on the other hand, for a limit cycle or periodic attractor, the projected network will be ring, with a number of nodes equal to the period of the cycle. The former case corresponds to $D_0 = d$, and the latter to $D_0 = 1$.

## IV. RELATING TOPOLOGY WITH MULTIFRACTALITY

In the case of a multifractal time series, the topology of the associated undirected transition network described above, in particular its degree distribution, can be related to the generalized dimensions $D_q$. We will consider in particular the degree distribution $P_\varepsilon(k)$ of a projected network with a coarse-graining level $\varepsilon$, defined as the probability that a randomly chosen node has degree $k$, i.e., it is connected to $k$ other nodes. To make explicit this relation, we observe that every node (box) $i$, will be characterized by a number of visits $n_i$ and a degree $k_i$. In the limit $n \to \infty$, we assume that the relative number of visits, i.e., the natural measure $p_i(\varepsilon)$, and the degree of a node are stable quantities. The corresponding

degree distribution will thus depend only on the phase space discretization $\varepsilon$. On average, the two quantities $p_i(\varepsilon)$ and $k_i$ will be related, since obviously the more times a box is visited, the larger is expected to be the degree of the associated node. We can thus assume a functional relation between these two averaged quantities, valid for sufficiently large $k_i$ and $p_i$, of the form

$$p_i(\varepsilon) \simeq G_\varepsilon(k_i), \tag{7}$$

where $G_\varepsilon(z)$ is an increasing function of $z$. The function $G_\varepsilon(k_i)$ depends in general on $\varepsilon$. Indeed, from the normalization of the natural measure, Eq. (7) implies that

$$\sum_i G_\varepsilon(k_i) \equiv N(\varepsilon) \sum_k P_\varepsilon(k) G_\varepsilon(k) = N(\varepsilon)\langle G_\varepsilon(k)\rangle = 1,$$

where we have defined $\langle F(k)\rangle = \sum_k P_\varepsilon(k)F(k)$. From here, we have

$$\langle G_\varepsilon(k)\rangle = N(\varepsilon)^{-1} \sim \varepsilon^{D_0}. \tag{8}$$

We make the assumption, to be validated numerically later on, that the $\varepsilon$ dependence of the function $G_\varepsilon(k)$ resides exclusively in a multiplicative prefactor, i.e., $G_\varepsilon(k) = a(\varepsilon)g(k)$. From Eq. (8), we have that $\langle G_\varepsilon(k)\rangle = a(\varepsilon)\langle g(k)\rangle \sim \varepsilon^{D_0}$. We make the additional assumption that the average of $g(k)$, $\langle g(k)\rangle$, is a constant, independent of $\varepsilon$. From here, we obtain the relation

$$p_i(\varepsilon) \simeq \varepsilon^{D_0}\, g(k_i). \tag{9}$$

This relation implies that we can express the multifractal properties of the attractor in terms of topological properties of the network. In fact, from Eq. (9), we have

$$\sum_i p_i(\varepsilon)^q \simeq \sum_i [\varepsilon^{D_0} g(k)]^q \simeq \varepsilon^{qD_0} N(\varepsilon) \sum_k P_\varepsilon(k) g(k)^q$$
$$\simeq \varepsilon^{(q-1)D_0} \langle g(k)^q\rangle, \tag{10}$$

where we have used $N(\varepsilon) \sim \varepsilon^{-D_0}$. From Eq. (6) we have also $\sum_i p_i(\varepsilon)^q \sim \varepsilon^{(q-1)D_q}$. Combining this with Eq. (10), we obtain the relation linking network and multifractal properties, namely,

$$\langle g(k)^q\rangle \sim \varepsilon^{-(q-1)(D_0-D_q)}. \tag{11}$$

For a homogeneous fractal set, $D_q = D_0\ \forall q$, and $\langle g(k)^q\rangle =$ const. On the other hand, for a multifractal strange attractor, since $D_q < D_0$ for $q > 0$, we have that the moments $\langle g(k)^q\rangle$, with $q > 1$, diverge as the number of boxes in the partition increases, i.e., as the network size grows. This observation allows to extract conclusions on the functional form of the degree distribution, which will depend on the particular growth law $g(k)$. We will consider analytically tractable forms in the following section. To avoid complications in the development, we will further assume in our analysis that the degree distribution of the projected network is stable, meaning that the effect of $\varepsilon$ consists essentially in imposing an upper degree cutoff $k_c$ to a functional form $P(k)$ independent of $\varepsilon$.

### A. Exponential growth

Let us consider first the case of an exponential (faster than algebraic) growth of the number of visits in a box with the associated node degree, i.e.,

$$g(k) \sim e^{\beta k}, \tag{12}$$

where $\beta > 0$. The fact that $\langle e^{\beta k}\rangle$ is constant and $\langle e^{\beta q k}\rangle$ diverges for $q > 1$ is compatible with a degree distribution that shows, at large values of $k$, the asymptotic behavior $P(k) \sim e^{-\alpha k}$, with $\alpha > \beta$, that is, an exponentially bounded degree distribution. Assuming a stable degree distribution, for a nonzero $\varepsilon$ the divergence of the exponential moments $\langle e^{\beta q k}\rangle$ will be reflected in a dependence on the network size $N(\varepsilon)$, modulated by the largest degree in the network, or degree cutoff $k_c(\varepsilon)$ [28]. To estimate this value, we observe that, from Eq. (9), $k_i \sim \ln[p_i(\varepsilon)/\varepsilon^{D_0}]^{1/\beta} \sim \ln[\varepsilon^{-(D_0-\alpha_i)/\beta}]$. The largest value of $k_i$ will correspond to the minimum of $\alpha_i$, $\alpha_{\min} = D_\infty$. Therefore, we have

$$k_c(\varepsilon) \sim \ln[\varepsilon^{-(D_0-D_\infty)/\beta}]. \tag{13}$$

This expression allows us to relate the network parameters $\alpha$ and $\beta$ with the multifractal exponents $D_0$ and $D_\infty$ by noticing that, in a network of finite size $N(\varepsilon)$, the maximum degree is given by the condition $\sum_{k=k_c(\varepsilon)}^{\infty} P(k) = 1/N(\varepsilon)$ [28]. With an exponential degree distribution $P(k) = \alpha e^{-\alpha k}$, we thus have, in the continuous degree approximation, $\int_{k_c(\varepsilon)}^{\infty} \alpha e^{-\alpha k}\, dk = e^{-\alpha k_c(\varepsilon)} = 1/N(\varepsilon)$, from where we obtain

$$k_c(\varepsilon) \sim \ln[N(\varepsilon)^{1/\alpha}] \sim \ln[\varepsilon^{-D_0/\alpha}]. \tag{14}$$

Combining Eqs. (13) and (14), we obtain the relation

$$\frac{\alpha}{\beta} = \frac{D_0}{D_0 - D_\infty}. \tag{15}$$

The properties of the network can also be used to extract information on the full set of generalized dimension by building on relation Eq. (11). Indeed, we can write the diverging moments in a finite network as

$$\langle e^{\beta q k}\rangle \sim \int^{k_c(\varepsilon)} e^{(q\beta-\alpha)k}\, dk \sim \frac{e^{(q\beta-\alpha)k_c(\varepsilon)}}{q\beta - \alpha}, \tag{16}$$

which, taking into account Eq. (13), yields

$$\langle e^{\beta q k}\rangle \sim \varepsilon^{-(D_0-D_\infty)(q-\alpha/\beta)}. \tag{17}$$

Combining Eq. (17) and Eq. (11) leads to the asymptotic expression, valid for large $q$,

$$D_q \sim D_\infty \frac{q}{q-1}, \tag{18}$$

which recovers the result known for deterministic multifractal measures [24].

### B. Algebraic growth

In the case of an algebraic growth of the number of visits with the associated degree, we have

$$g(k) \sim k^\delta, \tag{19}$$

with $\delta > 0$. From Eq. (11), we have that $\langle k^\delta\rangle$ is finite, and $\langle k^{q\delta}\rangle$, with $q > 1$, diverge in the limit of infinite network size. The fact that all higher degree moments diverge indicate that the degree distribution $P(k)$ of the network has long tails, which in the simplest case are compatible with a power-law distribution

of the form $P(k) \sim k^{-\gamma}$, where we impose $\gamma > \delta + 1$ to ensure a finite value of $\langle k^{\delta} \rangle$.

Performing again a finite-size analysis, from Eq. (9) we obtain a maximum degree,

$$k_c(\varepsilon) \sim \varepsilon^{-(D_0 - D_\infty)/\delta} \sim N(\varepsilon)^{(1 - D_\infty/D_0)/\delta}. \quad (20)$$

On the other hand, the network relation $\sum_{k=k_c(\varepsilon)}^{\infty} P(k) = 1/N(\varepsilon)$ leads now, with a power-law degree distribution $P(k) \sim k^{-\gamma}$ in the continuous degree approximation, to [28]

$$k_c(\varepsilon) \sim N(\varepsilon)^{1/(\gamma-1)} \sim \varepsilon^{-D_0/(\gamma-1)}. \quad (21)$$

Combining Eqs. (20) and (21), we obtain the relation between network properties and multifractal exponents:

$$\frac{\gamma - 1}{\delta} = \frac{D_0}{D_0 - D_\infty}. \quad (22)$$

In the case of an algebraic $g(k)$ function, Eqs. (20) and (21) can be used to directly estimate $\delta$ and $\gamma$. This approach is more difficult in the case of an exponential $g(k)$, due to the much smaller range of variation of the logarithm of $\varepsilon$; see Eqs. (13) and (14).

Finally, writing

$$\langle k^{\delta q} \rangle \sim \int^{k_c(\varepsilon)} k^{\delta q - \gamma}\, dk \sim k_c(\varepsilon)^{\delta q - \gamma + 1} \sim \varepsilon^{-D_0[\delta q/(\gamma-1) - 1]}, \quad (23)$$

and comparing with Eq. (11), we obtain again the simple asymptotic expression for the generalized dimensions given by Eq. (18).

## V. NUMERICAL EXPERIMENTS

In order to check the validity of the predictions made in Sec. IV, we have considered different multifractal time signals, generated by means of iterative maps. In particular, we have studied three paradigmatic examples of one- and two-dimensional chaotic attractors, namely the logistic, the Duffing, and the Henon map. The well-known logistic recurrence [6,29] in dimension $d = 1$,

$$x_{t+1} = \mu\, x_t (1 - x_t), \quad (24)$$

maps the interval $x \in [0,1]$ into itself when the control parameter $\mu$ ranges between 0 and 4. This system undergoes a period-doubling bifurcation transition to chaos, which sets-in at $\mu = 3.569456\ldots$. Multifractal chaotic regimes interspersed with periodic windows then occur in the parameter interval $\mu \in [3.57,4)$. Here we fix $\mu = 3.7$. The two-dimensional Duffing map,

$$x_{t+1}^{(1)} = x_t^{(2)}, \quad (25)$$

$$x_{t+1}^{(2)} = -b\, x_t^{(1)} + a\, x_t^{(2)} - \left[x_t^{(2)}\right]^3, \quad (26)$$

is a discrete representation of the Duffing oscillator, describing a forced oscillator coupled to a dissipative restoring force [6]. This map typically produces chaotic behaviors with the critical parameters $a = 2.75$ and $b = 0.2$, and generates values of $x^{(1)}$ and $x^{(2)}$ in the range $[-1.71,1.71]$. Following our network projection algorithm, each variable is thus shifted and normalized into the interval $[0,1]^2$.

Finally, the Henon map [6,30] in $d = 2$ is defined by the recurrence

$$x_{t+1}^{(1)} = 1 - a\left[x_t^{(1)}\right]^2 + x_t^{(2)}, \quad (27)$$

$$x_{t+1}^{(2)} = b\, x_t^{(2)}, \quad (28)$$

with the parameters $a$ and $b$ fixed to 1.4 and 0.3, respectively. For these values, starting from an initial point $(x_0^{(1)}, x_0^{(2)})$, the dynamics can either asymptotize to a fractal attractor relying on the subset $x^{(1)} \in [-1.3,1.3]$ and $x^{(2)} \in [-0.4,0.4]$ or diverge to infinity. For other values of $a$ and $b$ the map may be still chaotic, intermittent, or converge to a periodic orbit. Here we use the classical parameter setting and, again, we transform the values of each variable into the interval $[0,1]^2$. A one-dimensional projection of the Henon map is also considered, obtained by taking into account only one normalized variable of the map (both $x^{(1)}$ and $x^{(2)}$ give analogous results).

In Table I we present a summary of the multifractal properties of the chaotic time signals considered, computed by using the box counting formalism described in Sec. II. In particular, from Eq. (6), we compute the exponent $D_q$ by performing a linear regression of $\log \sum_i p_i(\varepsilon)$ as a function of $\log \varepsilon$, for $\varepsilon = M^{1/d}$, in a range of values of $M$ between $10^3$ and $4 \times 10^6$, depending of the particular attractor. The slope of this regression yields the factor $(q-1)D_q$. According to Eq. (18), the asymptotic value $D_\infty$ is obtained by means of linear regressions of $D_q$ as a function of $q/(q-1)$, performed over suitable intervals of the variable $q/(q-1)$. In Fig. 1 we present numerical data for $D_q$ as a function of $q/(q-1)$ for $q$ ranging between 30 and 80, computed using ensembles of 100 signals of length $n = 10^3 \times M$ iterations, with different seeds.

In Fig. 2 we plot the natural measure $\bar{p}_\varepsilon(k)$, averaged over all nodes of degree $k$, as a function of $k$, for different partitions of the multifractal attractors, i.e., different $\varepsilon$ (or $M$). In order to check the main assumption in Eq. (9), we plot the rescaled function $\varepsilon^{-D_0}\, \bar{p}_\varepsilon(k)$ as a function of the degree, using the fractal dimensions $D_0$ quoted in Table I. In this case, we expect all plots of each map for different $\varepsilon$ to collapse onto the single universal function $g(k)$. From Fig. 2 we observe,

TABLE I. Properties of the different multifractal maps and associated projected undirected and unweighted networks.

| Attractor | $d$ | $D_0$ | $D_\infty$ | $\beta$ | $\delta$ | $\alpha$ | $\gamma$ |
|---|---|---|---|---|---|---|---|
| Logistic | 1 | 0.998(2) | 0.49(1) | – | 1.04(2) | – | 3.14(1) |
| Duffing | 2 | 1.306(2) | 0.75(1) | 0.28(8) | – | 0.42(6) | – |
| Henon | 1 | 1.000(1) | 0.73(2) | – | 1.10(5) | – | 4.48(1) |
| | 2 | 1.24(1) | 0.82(2) | 0.15(2) | – | 0.57(5) | – |

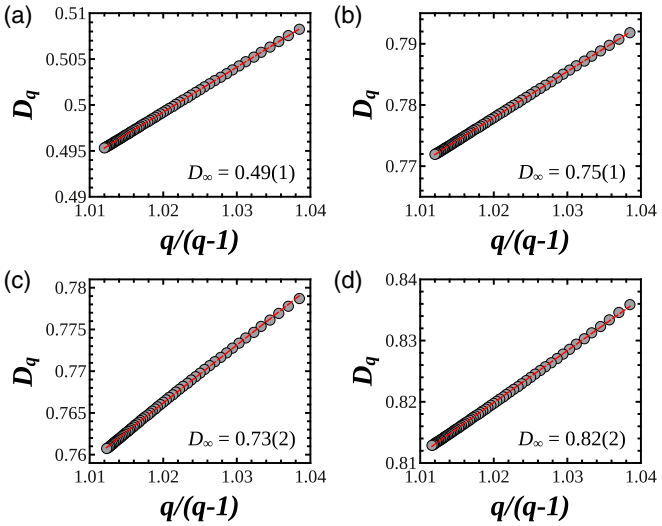


FIG. 1. Generalized dimensions $D_q$ as a function of $q/(q-1)$ for the logistic map (a), the Duffing map (b), the $d = 1$ Henon map (c), and the $d = 2$ Henon map (d). Error bars are smaller than the symbol sizes. The corresponding asymptotic values of $D_\infty$ can be extrapolated by means of a linear regression of these plots following Eq. (18). The results are listed in Table I.

for the logistic, Duffing and $d = 2$ Henon maps, a perfect convergence of the rescaled average natural measure as a function of $k$, indicating the validity of the assumption in Eq. (9). In the case of the $d = 1$ projection of the Henon attractor, however, the collapse of $\bar{p}_\varepsilon(k)$ is not fulfilled. In this particular case, therefore, the predictions made in Sec. IV are not expected to hold.

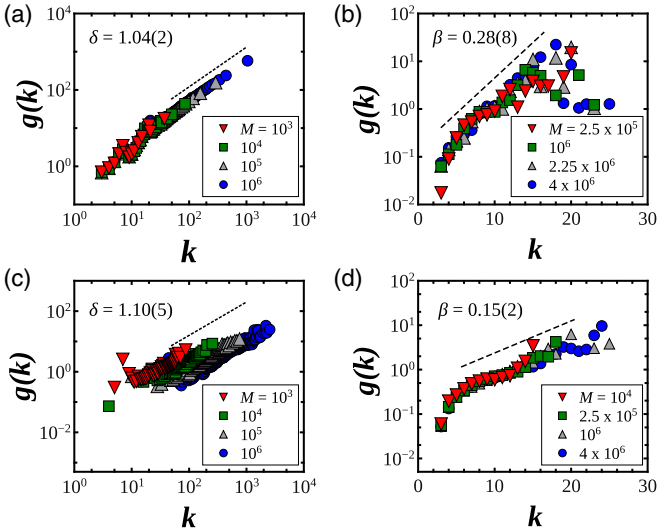


FIG. 2. Rescaled average natural measure, $\varepsilon^{-D_0}\bar{p}(k)$, as a function of the degree $k$ for the logistic map (a), the Duffing map (b), the $d = 1$ Henon map (c), and the $d = 2$ Henon map (d). The function $\bar{p}(k)$ is computed for different values of $M$, considering $n = 1000 \times M$ iterations. Dashed lines represent the estimated values of the exponents $\delta$ or $\beta$ in each case; see Table I.

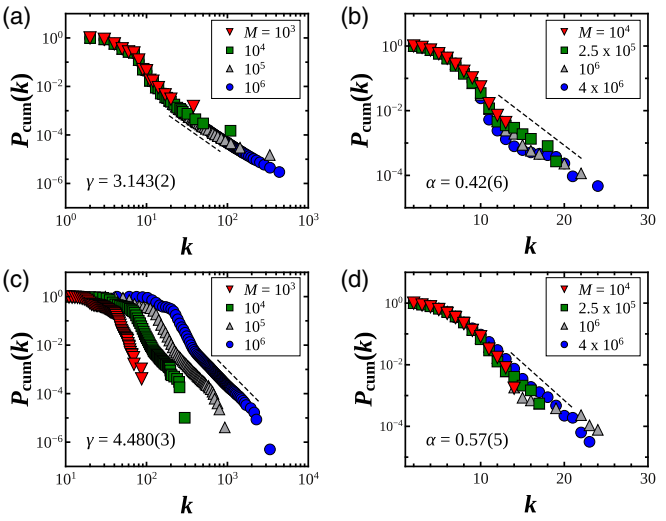


FIG. 3. Complementary cumulative degree distributions, $P_{\text{cum}}(k)$ of the undirected networks projected from the logistic map (a), the Duffing map (b), the $d = 1$ Henon map (c), and the $d = 2$ Henon map (d), computed for different values of $M$ and with $n = 1000 \times M$ iterations. Dashed lines represent the estimated values of $\gamma$ or $\alpha$ of the pertinent case; see Table I.

From Fig. 2, we also observe that in the $d = 1$ cases [Figs. 2(a) and 2(c)], both the attractor of the logistic map and that of the projected Henon map obey an algebraic behavior, $g(k) \sim k^\delta$, while in the $d = 2$ cases [Figs. 2(b) and 2(d)], both the Duffing and the Henon systems show an exponential growth, $g(k) \sim e^{\beta k}$. A linear regression performed on the data of the log-log plot in Fig. 2 provides an estimation of the exponents $\delta$ and $\beta$. In general, it can be noticed how these linear trends become more defined and stable while refining the statistics of $g(k)$ by increasing $M$; we thus fit data obtained with $M = 10^6$ in the algebraic case and $M = 4 \times 10^6$ for an exponential $g(k)$. We find the exponents $\delta = 1.04(2)$ for the logistic map, $\beta = 0.28(8)$ for the Duffing map, while $\delta = 1.10(5)$ and $\beta = 0.15(2)$ are obtained for the $d = 1$ and the $d = 2$ Henon maps, respectively.

In Fig. 3 we examine the topology of the projected networks by plotting the complementary cumulative degree distributions, $P_{\text{cum}}(k) = \sum_{q=k}^{\infty} P(q)$, for different values of $M$. As predicted in Sec. IV, the networks characterized by an algebraic growth $g(k)$ (here $d = 1$ cases) exhibit power-law degree distributions. Figures 3(a) and 3(c) show how for different network sizes (i.e., different values of $M$) all trends converge to a common power-law distribution characterized by $\gamma = 3.14(1)$ in the logistic networks and $\gamma = 4.48(1)$ for the $d = 1$ Henon networks. Interestingly, in this last case, the prediction of a scale-free degree distribution holds, despite the fact that Eq. (9) is not fulfilled. This must be attributed to the affect of an algebraic function $g(k)$, still present in the $d = 1$ Henon map. By contrast, the networks resulting from the projection of the $d = 2$ maps follow short-tailed degree distributions, compatible with an exponential behavior $P(k) \sim e^{-\alpha k}$. These plots present a poor statistics and we can only extrapolate rough values for $\alpha$, namely $\alpha = 0.42(6)$ and $\alpha = 0.57(5)$ for the Duffing and $d = 2$ Henon maps, respectively.

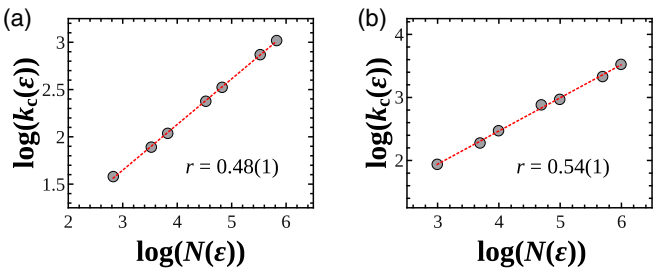


FIG. 4. Scaling of the degree cutoff, $k_c(\epsilon)$, estimated as the maximum degree in the network, as function of the network size $N(\epsilon)$ for the logistic map (a), and the $d = 1$ Henon map (b). The logarithms in figure are in base 10.

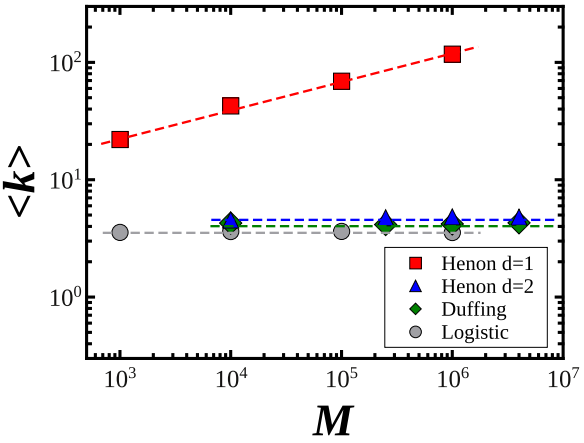


FIG. 5. Average degree, $\langle k \rangle$, as a function of $M$ for the different maps considered. All of them, except for the $d = 1$ projection of the Henon map are essentially independent of the network discretization.

With these values characterizing the multifractal properties of the maps and the topological properties obtained from the analysis of the projected transition networks, we can validate our theoretical framework. We first check the cross-relations given by Eqs. (15) and (22) for exponential and algebraic cases, respectively. Regarding the algebraic examples we obtain $(\gamma - 1)/\delta = 2.06(7)$ and $D_0/(D_0 - D_\infty) = 1.96(5)$ for the logistic map (see values from Table I). In this case, the identity Eq. (22) is well fulfilled within error bars. For the Henon attractor in $d = 1$, we obtain instead $(\gamma - 1)/\delta = 3.2(2)$ and $D_0/(D_0 - D_\infty) = 3.7(3)$, again coinciding within error bars. For exponential cases, the equality Eq. (15) leads to the comparison $\alpha/\beta = 1.5(6)$ and $D_0/(D_0 - D_\infty) = 2.34(5)$ for the Duffing map, and $\alpha/\beta = 3.8(8)$ and $D_0/(D_0 - D_\infty) = 2.9(2)$ for the $d = 2$ Henon attractor. In this case, the exponent relations are affected by stronger errors, but the trend is clearly toward a positive comparison.

Finally, for an algebraic $g(k)$, as observed in the logistic map and the $d = 1$ projection of the Henon attractor, we can proceed to check the behavior of the maximum degree $k_c(\varepsilon)$ as a function of the network size $N(\varepsilon)$, see Fig. 4. We do not consider the relation between degree cutoff and network size for maps with an exponential $g(k)$, since the very small span of network sizes obtained does not allow for a determination of the exponent in relation Eq. (13). Indeed, for the algebraic case, following Eq. (20), the behavior of the maximum degree is given by $k_c(\varepsilon) \sim N(\varepsilon)^r$, with the exponent $r = (1 - D_\infty/D_0)/\delta$. The numerical exponents obtained through a linear regression of $\log k_c(\varepsilon)$ as a function of $\log N(\varepsilon)$ are $r = 0.48(1)$ and $r = 0.54(1)$ for the logistic and the $d = 1$ Henon map, respectively. From the values of $\delta$, $D_0$ and $D_\infty$ in Table I, our theoretical predictions are $r = 0.48(3)$ and $r = 0.25(3)$ for the logistic and the $d = 1$ Henon map, respectively. The agreement between numerics and theory is very good for the logistic map, but completely off in the $d = 1$ Henon case. The disagreement in this last case must be attributed to the failure of Eq. (9). While the general shape of $P(k)$ compatible with a power-law is ensured by the algebraic form of $g(k)$, the lack of its expected dependence on the prefactor $\varepsilon$ (see Fig. 2) affects the scaling relations deduced from Eq. (9). In the $d = 1$ Henon case yet another of the approximations made breaks down, namely the assumption of a stable degree distribution. This fact is further checked in Fig. 5, which shows that the average degree $\langle k \rangle$ of the projected networks is essentially independent of $\varepsilon$ for all the multifractal time signals considered, except for the $d = 1$ Henon attractor, which exhibits instead a power-law increasing behavior. This fact indicates that $d = 1$ Henon networks belong to the class of accelerated networks [31]. This increasing average degree prevents the degree distribution to be stable, introducing an additional scale, beyond the degree cutoff $k_c$. Surprisingly, however, the exponent relation Eq. (22) seems to still be fulfilled, at least within error bars.

## VI. WEIGHTED UNDIRECTED NETWORK PROJECTIONS

The transition networks discussed above have been considered as undirected and binary, meaning that there is a single edge between nodes $i$ and $j$ if there has been at least a transition between boxes $i$ and $j$, irrespective of the order it occurs. This restriction can, however, be lifted by considering the more general cases of weighted or directed transition networks. In an undirected weighted transition network [19,21,32,33], a weight $\omega_{ij}$, given by a real number, is associated to the edge joining nodes $i$ and $j$. In a transition network framework, the natural choice is to make $\omega_{ij}$ equal to the number of transitions $n_{ij}$ between boxes $i$ and $j$, irrespective of their directionality. We therefore associate to each edge the normalized weight

$$\omega_{ij} = \frac{n_{ij}}{n}. \tag{29}$$

The statistical pattern of weights can be studied in terms of the weight distribution, $P(\omega)$, defined as the probability that a randomly chosen edge has weight $\omega$. This distribution cannot be simply related to the mutifractal spectrum of a time series, since this spectrum disregards the transitions between different boxes. In Fig. 6 we plot the complementary cumulative weight distributions $P_{\rm cum}(\omega) = \sum_{\omega'=\omega}^{\infty} P(\omega')$ obtained numerically from the different maps we analyzed above. As we can see, in all cases we obtain long-tailed distributions, that can be approximated to a power-law form $P(\omega) \sim \omega^{-a}$, with an exponent $a$ between 3 and 4 (see Table II).

An important measure in weighted networks is the vertex strength $s_i$ [32,33], defined as the sum of all weights incident

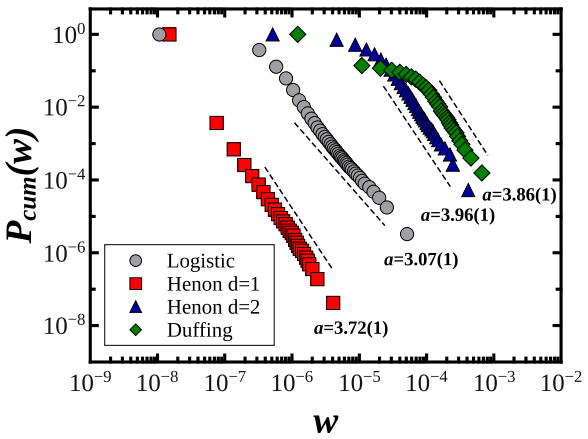


FIG. 6. Complementary cumulative weight distributions, $P_{\rm cum}(\omega)$, of the weighted networks projected from the different maps, computed for $M = 10^6$ and $n = 10^9$. Dashed lines represent the estimated values of the exponent $a$, in a fit to the form $P(\omega) \sim \omega^{-a}$.

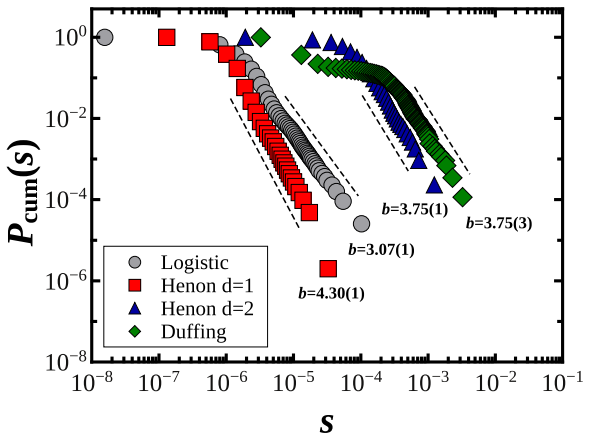


FIG. 7. Complementary cumulative strength distribution, $P_{\rm cum}(s)$, of the weighted networks projected from the logistic map (a), the Duffing map (b), the $d = 1$ Henon map (c), and the $d = 2$ Henon map (d), computed for $M = 10^6$ and $n = 10^9$. Dashed lines represent the estimated values of the exponent $b$, in a fit to the form $P(s) \sim s^{-b}$.

on vertex $i$, i.e.,

$$s_i = \sum_{j \in \mathcal{V}(i)} \omega_{ij}, \tag{30}$$

where $\mathcal{V}(i)$ is the set of neighbors of vertex $i$. Given the definition of the weights in Eq. (29), we have $s_i = 2n_i/n \equiv 2p_i(\varepsilon)$, i.e., proportional to the natural measure at box $i$. Therefore, the strength and natural measure distributions are identical, except for a trivial factor 2. In Fig. 7 we plot the complementary cumulative strength distributions, $P_{\rm cum}(s)$, computed for the four different considered maps. Once more, in all cases we observe a power-law distribution, $P(s) \sim s^{-b}$, with an exponent $b$ ranging between 3 and 5; see Table II.

The correlations between the pattern of weights and the topology of the network is usually determined by looking at the average strength of nodes of degree $k$, $\bar{s}(k)$ [33]. Given the relation between strength and natural measure, we can approximate [see Eq. (9)],

$$\bar{s}(k) \simeq 2\varepsilon^{D_0} g(k). \tag{31}$$

From the results in Fig. 2, we obtain $\bar{s}(k) \sim k^{\delta}$ for the $d = 1$ maps and $\bar{s}(k) \sim e^{\beta k}$ for the $d = 2$ maps. This allows to tie strength and degree distributions through the relation $P(s)ds = P(k)dk$, which, for the maps in $d = 1$, leads to the exponent relation

$$\gamma = \delta(b - 1) + 1. \tag{32}$$

Applying Eq. (32) and the values in Table II to the $d = 1$ maps, we obtain a satisfactory matching with the values extrapolated by fitting the unweighted degree distributions $P(k)$. In detail, we find $\gamma = 3.15(5)$ versus 3.14(1) for the logistic map and $\gamma = 4.6(2)$ versus 4.48(1) for the $d = 1$ Henon map.

Additionally, by combining Eq. (32) with Eq. (22), we obtain a relation between the exponent of the strength distribution and the multifractal spectrum, given by

$$b = 1 + \frac{D_0}{D_0 - D_\infty}. \tag{33}$$

For the $d = 2$ maps with an exponential growth of $g(k)$, the combination with a power-law strength distribution leads to an exponential degree distribution, $P(k) \sim e^{-\alpha k}$, in agreement with the results presented above, with

$$\alpha = \beta(b - 1). \tag{34}$$

Toward a favorable comparison, though less quantitative as compared to $d = 1$ cases, are also these exponents obtained for the $d = 2$ maps, namely $\alpha = 0.8(2)$ versus 0.42(6) for the Duffing map and $\alpha = 0.41(6)$ versus 0.57(5) for the $d = 2$ Henon map.

Comparison of Eq. (34) with Eq. (15) leads again to Eq. (33), relating $b$ with the multifractal spectrum. Application of Eq. (33) with the data of the multifractal analysis from Table I gives exponents $b = 2.96(5)$, 3.35(5), 4.7(3), and 4.0(2) for the logistic, Duffing, and $d = 1$ and $d = 2$ Henon maps, in reasonable agreement with the values extracted from a direct fit to the strength distribution; see Table II.

TABLE II. Properties of the different multifractal maps and associated projected undirected and weighted networks.

| Attractor | $d$ | $a$ | $b$ |
|---|---|---|---|
| Logistic | 1 | 3.07(1) | 3.07(1) |
| Duffing | 2 | 3.86(1) | 3.75(1) |
| Henon | 1 | 3.72(1) | 4.30(1) |
| | 2 | 3.96(1) | 3.75(3) |

## VII. DIRECTED NETWORK PROJECTIONS

Apart from a weighted projection, we can additionally consider a directed transition network projection, in which a directed edge pointing from node $i$ to node $j$ indicates the presence of a dynamical transition from box $i$ to box $j$ [19,21].

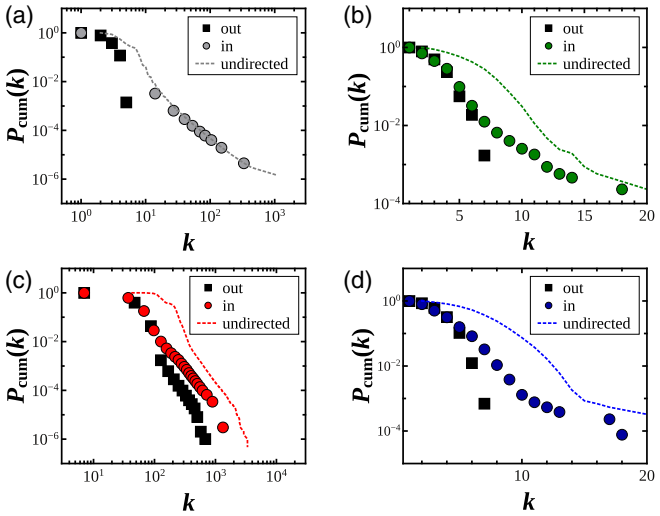


FIG. 8. Complementary cumulative in-degree and out-degree distributions of the directed networks projected from the logistic map (a), the Duffing map (b), the $d = 1$ Henon map (c) and the $d = 2$ Henon map (d), computed for $M = 10^6$ and $n = 10^9$. For the sake of comparison, in a dashed line we plot the degree distribution of the corresponding undirected network projection.

The topology properties of nodes in this (unweighted) directed network can be represented in terms of the in-degree $k_i^{\text{in}}$ and out-degree $k_i^{\text{out}}$ of node $i$, defined as the number of directed edges arriving to node $i$ and departing from node $i$, respectively [1].A statistical characterization of these quantities is given by the in-degree $P(k^{\text{in}})$ and out-degree $P(k^{\text{out}})$ distributions, measuring the probability that a randomly chosen node has in-degree $k^{\text{in}}$ or out-degree $k^{\text{out}}$, respectively. Information about these distributions cannot be obtained analytically, since the formalism developed above relies on the natural measure, which does not take transition directionality into account. We thus plot these distributions evaluated numerically in Fig. 8 for the different iterative maps under consideration. We observe that, in general, the span of the out-degree distributions is shorter than the one of the in-degree distributions, indicating that the out-degree of these networks is very homogeneous. This is specially evident in the logistic map, where the in-degree distribution shows a power-law tail, overlapping with the undirected degree distribution, while the out-degree distribution shows a strong exponential decay. For the $d = 1$ Henon map, both in- and out-degree distribution show power-law tails, compatible with the undirected degree distribution. For the case of the $d = 2$ maps, Duffing and Henon, the in- and out-degree distributions are both exponential, like the undirected degree distributions, but all three appear to be different in both cases.

## VIII. DISCUSSION

In this paper, we have investigated the effect of fractal and multifractal properties of a temporal signal on the topology of the corresponding projected network. By combining a transition network representation with the box-counting formalism, we have mapped temporal signals into undirected unweighted networks whose nodes are the boxes partitioning the attractor of the temporal signal in the phase space, and links are established between successive pair of boxes between which the signal jumps. We have developed a mathematical framework connecting the network topology to the multifractal properties of the generating signal. This formalism allows us to predict the functional form of the network degree distribution on the basis of the functional, $g(k)$, linking the natural measure of a box with the associated node degree. We have focused on the prototypical and general cases of an exponential and an algebraic growth $g(k)$, showing that the latter results in power-law degree distributions whose exponent $\gamma$ is controlled by the multifractal exponents of the generating signal. We have verified the validity of our approach through extensive numerical simulations, highlighting the excellent agreement observed in many cases, and discussing in detail the reasons why in some cases (e.g., the Henon map in $d = 1$) the numerical experiments depart from some theoretical predictions.

In particular, we could conclude that a sufficient condition to obtain a scale-free topology is that the natural measure of a box must increase with the degree of the associated node in a algebraic fashion. In our numerical experiments we have observed that this condition is fulfilled in multifractal attractors in $d = 1$ with capacity dimension $D_0 = 1$. This fact leads us to conjecture that scale-free networks can be observed in general multifractal time series in which the capacity dimension is equal to the euclidean dimension of the embedding phase space.

We have additionally considered numerically the properties of weighted and directed versions of the projected network. In the case of weighted networks, a relation with the multifractal spectrum of the time series can be drawn at the level of the strength distribution and the strength correlations with the node's degree, giving rise to further information on the projected network structure. This analysis constitutes the basis for building new statistical tools for unravelling intrinsic directional constraints and correlations in multifractal dynamics.

Our work extends existing approaches bridging time series analysis and network science by addressing the ubiquitous case of signals exhibiting multifractal properties. By doing this, it enriches the set of interpretative tools available for a better characterization of empirical time-series. Viceversa, our approach also paves the way for exploiting multifractal generators as possible mechanisms for growing complex networks.

For this reason, we can envisage that it will be of interest also to the growing community of interdisciplinary researchers studying natural time series through the lenses of network science.

## ACKNOWLEDGMENTS

M.A.B. acknowledges financial support from FRS-FNRS. R.P.-S. acknowledges financial support from the Spanish MINECO, under Projects No. FIS2013-47282-C2-2 and No. FIS2016-76830-C2-1-P, and EC FET-Proactive Project MULTIPLEX (Grant No. 317532). R.P.-S. acknowledges additional financial support from ICREA Academia, funded by the Generalitat de Catalunya.

[1] M. E. J. Newman, *Networks: An Introduction* (Oxford University Press, Oxford, 2010).

[2] A. Barrat, M. Barthélemy, and A. Vespignani, *Dynamical Processes on Complex Networks* (Cambridge University Press, Cambridge, 2008).

[3] S. N. Dorogovtsev, A. V. Goltsev, and J. F. F. Mendes, Rev. Mod. Phys. **80**, 1275 (2008).

[4] R. Pastor-Satorras, C. Castellano, P. Van Mieghem, and A. Vespignani, Rev. Mod. Phys. **87**, 925 (2015).

[5] J. Guckenheimer and P. Holmes, *Nonlinear Oscillations, Dynamical Systems, and Bifurcations of Vector Fields* (Springer, New York, 2002).

[6] E. Ott, *Chaos in Dynamical Systems* (Cambridge University Press, Cambridge, UK, 1993).

[7] R. V. Donner, M. Small, J. F. Donges, N. Marwan, Y. Zou, R. Xiang, and J. Kurths, Int. J. Bifurcation Chaos **21**, 1019 (2011).

[8] P. Li, J. Zhang, X.-K. Xu, and M. Small, Chin. Phys. Lett. **29**, 048903 (2012).

[9] L. Lacasa, B. Luque, F. Ballesteros, J. Luque, and J. C. Nuño, Proc. Natl. Acad. Sci. USA **105**, 4972 (2008).

[10] L. Lacasa and R. Toral, Phys. Rev. E **82**, 036120 (2010).

[11] J. Zhang and M. Small, Phys. Rev. Lett. **96**, 238701 (2006).

[12] Y. Yang and H. Yang, Physica A: Stat. Mech. Appl. **387**, 1381 (2008).

[13] Z. Gao and N. Jin, Phys. Rev. E **79**, 066303 (2009).

[14] N. Marwan, J. F. Donges, Y. Zou, R. V. Donner, and J. Kurths, Phys. Lett. A **373**, 4246 (2009).

[15] Z. Gao and N. Jin, Chaos **19**, 033137 (2009).

[16] R. V. Donner, Y. Zou, J. F. Donges, N. Marwan, and J. Kurths, New J. Phys. **12**, 033025 (2010).

[17] R. Xiang, J. Zhang, X.-K. Xu, and M. Small, Chaos **22**, 013107 (2012).

[18] G. Nicolis, A. Garcia Cantu, and C. Nicolis, Int. J. Bifurcation Chaos **15**, 3467 (2005).

[19] A. H. Shirazi, G. R. Jafari, J. Davoudi, J. Peinke, M. R. R. Tabar, and M. Sahimi, J. Stat. Mech.: Theory Exp. (2009) P07046.

[20] A. Campanharo, M. Sirer, R. Malmgren, F. Ramos, and L. Amaral, PLoS ONE **6**, e23378 (2011).

[21] X. Sun, M. Small, Y. Zhao, and X. Xue, Chaos **24**, 024402 (2014).

[22] T. C. Halsey, M. H. Jensen, L. P. Kadanoff, I. Procaccia, and B. I. Shraiman, Phys. Rev. A **33**, 1141 (1986).

[23] K. Falconer, *Fractal Geometry: Mathematical Foundations and Applications*, 2nd ed. (John Wiley & Sons, Chichester, 2003).

[24] J. Feder, *Fractals*, Physics of Solids and Liquids (Springer, New York, 1989).

[25] M. A. Budroni, V. Pilosu, F. Delogu, and M. Rustici, Chaos: Interdisc. J. Nonlin. Sci. **24**, 023117 (2014).

[26] M. A. Budroni, E. Tiezzi, and M. Rustici, Physica A: Stat. Mech. Appl. **389**, 3883 (2010).

[27] A.-L. Barabási and R. Albert, Science **286**, 509 (1999).

[28] M. Boguñá, R. Pastor-Satorras, and A. Vespignani, Euro. Phys. J. B **38**, 205 (2004).

[29] R. M. May, Nature **261**, 459 (1976).

[30] M. Hénon, Commun. Math. Phys. **50**, 69 (1976).

[31] S. N. Dorogovtsev and J. F. F. Mendes, Adv. Phys. **51**, 1079 (2002).

[32] A. Barrat, M. Barthélemy, R. Pastor-Satorras, and A. Vespignani, Proc. Natl. Acad. Sci. USA **101**, 3747 (2004).

[33] M. Barthélemy, A. Barrat, R. Pastor-Satorras, and A. Vespignani, Physica A **346**, 34 (2005).